Effect of Perpendicular Magnetic Field on Chaos in a Rotating Cavity Heated from Side

R. Prasad[†] and A. K. Singh

Department of Mathematics, Banaras Hindu University, Varanasi, India-221005

†*Corresponding Author Email: rajendrabhu108@gmail.com*

ABSTRACT

This paper presents chaotic behavior due to an applied perpendicular magnetic field on a rotating cavity heated from side using the theory of dynamical system. The solution to the non-linear problem is obtained by using a truncated Galerkin method to find a set of ordinary differential equation for the time evolution of the Galerkin amplitudes. The system of differential equations is solved by using the fourth-order Runge Kutta method. Below a certain critical value of the scaled Rayleigh number the unique motionless conduction solution is obtained. At slightly super-critical values of scaled Rayleigh numbers transition to chaotic solutions occurs via a Hopf bifurcation. The chaotic behaviour can be obtained faster for decreasing Hartmann number as well as increasing scaled Rayleigh number. Also variation in Nusselt number increases with increasing scaled Rayleigh number and decreasing Hartmann number.

NOMENCLATURE

Ar	aspect ratio of the cavity(dimensionless)		v	component of velocity in direction of y axis
H_0	applied magnetic flux		w	component of velocity in direction of z axis
Ha	Hartmann number(dimensionless)			
H_1	height of cavity		$\chi,\ \chi_1,\ , \chi_2,\ \chi_3$ eigenvalues	
g	gravitational acceleration			
L_1	width of cavity		α_T	thermal diffusivity
p	pressure		α	Thermal expansion coefficient
Pr	Prandtl number(dimensionless)		β	adverse temperature gradient
$\hat{e}_x$	unit vector in x direction		γ_1	constant used in Eq. 26 (dimensionless)
$\hat{e}_y$	unit vector in y direction		δ_2	constant used in Eq. 26 (dimensionless)
R	scaled Rayleigh number(dimensionless)		ζ	constant used in Eq. 26 (dimensionless)
Ra	Rayleigh number(dimensionless)		υ	kinematic viscosity
$Ra_{\omega o}$	centrifugal Rayleigh number due to offset distance (dimensionless)		ρ	density
			ρ_0	density
Ra_ω	centrifugal Rayleigh number due to horizontal location of cavity (dimensionless)		σ	electric conductivity (S/m, Siemens per meter or)
t	time		τ	scaled time
T	temperature		ω	angular velocity
ΔT	temperature difference between the walls		ψ	stream function
u	component of velocity in direction of x axis			

1. INTRODUCTION

The phenomenon of natural convection in the enclosures has received considerable attention in recent years because this phenomenon often affects the thermal performance in many engineering and scientific applications such as boilers, nuclear reactor systems, energy storage and conservation, fire control and chemical, food and metallurgical industries. Buoyancy driven flows are complex

because of essential coupling between the transport properties of flow and thermal fields. The problem of Rayleigh-Benard convection interacting with a magnetic field, which is called magnetoconvection, has been investigated by Chandrasekhar (1952) and showed that the magnetic flux was concentrated into sheets at the sides of the square cell, from which the motion was excluded. Lorenz (1963) found the route to chaos in a fluid layer and studied two dimensional fluid cell heated from below and cooled from above (also known as the Raleigh-Benard problem) in order to model unpredicted behaviour in the weather. He proposed the three-dimensional set of partial differential equations known as the model of the convection and suggested that it is difficult to reach good accuracy in very long range forecasting because this model gives rise to the chaotic behaviour. Greenspam (1980) presented the terms for the representation of the centrifugal and Coriolis forces due to the rotation in pure fluids.

Magnetoconvection has been investigated by Weiss 1981) as a result of numerical simulations of the partial differential equations for a two-dimensional Boussinesq magnetoconvection and showed that the magnetic flux was concentrated into sheets at the sides of the square cell. Knobloch *et al*. (1981, 83, 86) carried out numerical simulations of compressible three-dimensional magnetoconvection and showed complicated spatiotemporal behavior. Nonlinear modulational dynamics of travelling rolls in three-dimensional magnetoconvection was investigated near the onset of a Hopf bifurcation and criteria for the modulational instability of travelling rolls were obtained by means of the reductive perturbation method. It is not often possible to establish analytically the nature of chaotic solutions. In this situation, it is observed by solving numerically the partial differential equations. Rucklidge 1992) showed how the PDEs for a two dimensional Boussinesq convection in a vertical magnetic field could be reduced for a particular range of parameters, first to a third order set of ordinary differential equations and then to a one dimensional map. The analysis of the map shows an abrupt transition from periodic to chaotic behaviour. Rucklidge (1992) derived a third-order set of ordinary differential equations that governing the behavior of PDEs and found the first chaotic oscillations of the third-order system. Analytical solutions for the linear stability of free convection in a porous layer subject to rotation for the case when the temperature gradient resulting from the conditions imposed on the boundaries is collinear with the centrifugal body force were presented by Vadasz (1994) considering a porous layer which is placed in an arbitrary positive distance from the axis of rotation. The linear stability analysis provided the stability criteria, i.e., the critical centrifugal Rayleigh numbers, the critical wave numbers and the corresponding eigen functions for different values of the parameters controlling the offset distance from the axis of rotation, and allowed to describe qualitatively the convective flow. However, as usual, the linear stability analysis cannot provide information regarding the values of

the convection amplitudes nor regarding the average rate of heat transfer. Matsuba (1997) found an excitation of large-scale modulation of amplitude of two-dimensional Boussinesq magnetoconvection which was closely related to the excitation of the convective-cell modes in drift wave turbulence. Vadasz (1998) reported the results of non-linear solutions to this problem including possible transitions between different regimes of convection at supercritical values of the centrifugal Rayleigh number. Rucklidge (1994, 98, 2000) carried out the numerical simulations of compressible three dimensional magnetoconvection and showed complicated spatiotemporal behavior. Nonlinear modulational dynamics of travelling rolls in three-dimensional magnetoconvection was investigated near the onset of a Hopf bifurcation and criteria for the modulational instability of travelling rolls were obtained by means of the reductive perturbation method. Also Cox (2001) found an excitation of large-scale modulation of amplitude of two-dimensional Boussi-3 nesqagnetoconvection which was closely related to the excitation of the convective-cell modes in drift wave turbulence. In modeling such a system, several factors should be taken into account, in particular the inhomogeneity of the (strong) external magnetic field and the three-dimensionality of the enclosure. Moreover, the flow stabilization effect (connected with the external magnetic field) for the oscillatory flow of a liquid-metal in a laterally heated rectangular cavity was studied by Gelfgat and Bar-Yoseph (2001).

Chen and Price (2006) found a relation between the Rayleigh-Benard convectoin and Loentz system. Bekki and Moriguchi (2007) investigated chaos in the Boussinesq magnetoconvection with stress-free boundary conditions. Their results showed that the long-term behavior of the magneto-convection exhibits spatially coherent and temporally chaotic rolls, in marked contrast to the long-term behavior of highly turbulent fluids. Nithyadevi *et al*. (2007) studied natural convection in a rectangular cavity with partially active side walls. Kandaswamy *et al*. (2008) numerically investigated flow and temperature fields in a square cavity with partially active vertical walls for Prandtl number of water (7.0). The active part of the left side wall is at a higher temperature than the active part of the right side wall. The top, bottom and the inactive parts of the side walls are thermally inactive. They found that heat transfer rate is maximum for the middle thermally active locations while it is poor for the top-bottom thermally active locations. Recently, Prasad and Singh (2013) investigated the effect of perpendicular magnetic field on chaos in a cavity heated from below. The objective of this paper is to demonstrate the possible convection regimes at supercritical values of the Rayleigh number and also the effect of the perpendicular magnetic field on transition to chaos in a rotating cavity heated from side. The solution to the non-linear problem is obtained using the truncated Galerkin method that gives a set of ordinary differential equation for the time evolution of the Galerkin amplitudes.

2. PROBLEM FORMULATION

Here, the unsteady free convective flow of a viscous incompressible and electrically conducting fluid in cavity of length L and width H is considered. The x'-axis is taken along the bottom and y'-axis transverse to it having origin at the lower end of the left wall. A constant magnetic field H_0 is applied perpendicular to the cavity along z'-axis.
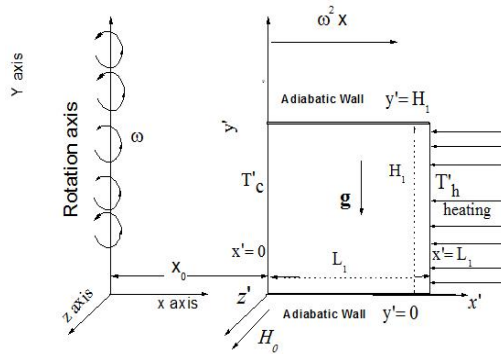
Fig. 1. Physical model and coordinate system.

The flow is assumed to be at small magnetic Reynolds number and hence the induced magnetic field can be neglected. The horizontal top and bottom walls are thermally insulated while the left and right walls of the cavity are maintained at isothermal but different temperature T_c' and, T_h' respectively. The viscous and Ohmic dissipation terms have been neglected. This cavity is subjected to rotation at distance x_0 from the axis of rotation as presented in Fig. 1. Two systems of coordinates are presented in Fig. 1, the first (X, Y, Z) is linked to the axis of rotation and the second (x', y', z'), placed a horizontal distance x_0, apart from the first one, belongs to the cavity coordinates. A positive temperature gradient along the *x*-axis is anticipated as a result of the imposed thermal boundary conditions. This temperature gradient is collinear with the centrifugal acceleration. The significance of the variation of the centrifugal acceleration in the *x* direction depends on the offset distance from the axis of rotation. For the layer of fluid in cavity which is adjacent to the rotation axis $(i.e., x_0 = 0)$ the variation of the centrifugal acceleration leads practically to a zero acceleration at X = 0 and a maximum value of acceleration at X = 1. The front aspect ratio of the cavity is defined as $Ar = H_1/L_1$, where H_1 and L_1, are the height and the length of the cavity, respectively. Free convection may occur as a result of the centrifugal body force while the gravity force is neglected. The condition for this assumption to be valid was developed by Vadasz (1996). In addition Govender (1995) and Greenspan (1980) showed that (in the corresponding problem of combined gravity and centrifugal buoyancy) the linear stability results, i.e. the critical value and the eigen-functions are identical to the problem where gravity effects are weak and therefore neglected. Here, inertial effects i.e. the centrifugal acceleration are considered as far

as change in the density and the Boussinesq approxi--imation is applied for the effects of density variations. Under these conditions the following set of governing equation (the unsteady, incmpressible Navier-Stokes equation) is obtained (see Greenspan (1980) for centrifugal term in the derivation of Eq. (2)) as

$$\nabla.\mathbf{q} = 0 \tag{1}$$

$$\frac{\partial \mathbf{q}}{\partial t} + (\mathbf{q}.\nabla)\mathbf{q} = -\frac{1}{\rho_0}\nabla p + \upsilon\nabla^2\mathbf{q}$$

$$+\frac{\rho}{\rho_0}(g\hat{e}_y + w^2 x\hat{e}_x) + \frac{\sigma}{\rho_0}[(\mathbf{q}\times\mathbf{H})\times\mathbf{H}] \tag{2}$$

$$\frac{\partial \mathbf{q}}{\partial t} + (\mathbf{q}.\nabla)T = \alpha_T\nabla^2 T. \tag{3}$$

By using the Boussinesq approximation, the governing equations - continuity, momentum and thermal energy in two dimensional forms, can be written as Eqs. (4 - 7)

$$\frac{\partial u'}{\partial x'} + \frac{\partial v'}{\partial y'} = 0 \tag{4}$$

$$\frac{\partial u'}{\partial t'} + u'\frac{\partial u'}{\partial x'} + v'\frac{\partial u'}{\partial y'} = -\frac{1}{\rho_0}\frac{\partial p'}{\partial x'}$$

$$+\upsilon\nabla^2 u' + \frac{\rho}{\rho_0}\omega^2(x_0' + x') - \frac{\sigma H_0^2}{\rho_0}u' \tag{5}$$

$$\frac{\partial v'}{\partial t'} + u'\frac{\partial v'}{\partial x'} + v'\frac{\partial v'}{\partial y'} = -\frac{1}{\rho_0}\frac{\partial p'}{\partial y'}$$

$$+\upsilon\nabla^2 v' - \frac{\sigma H_0^2}{\rho_0}v', \tag{6}$$

$$\frac{\partial T'}{\partial t'} + u'\frac{\partial T'}{\partial x'} + v'\frac{\partial T'}{\partial y'} = \alpha_T\nabla^2 T'. \tag{7}$$

Where u' and v' are the velocity components in the x'-axis and y'-axis directions, respectively, p' the pressure, T' the temperature, ν the kinematic viscosity, α_T the thermal diffusivity and σ the electrical conductivity. For the flow model considered, the boundary conditions for the velocity and temperature fields are given by

$$u' = v' = 0 \text{ at } x' = 0, L_1 \text{ and}$$

$$\text{at } y' = 0, H_1, \tag{8}$$

$$T' = T_c' \text{ at } x' = 0 \text{ and } T' = T_h' \text{ at } x' = L_1 \tag{9}$$

$$\frac{\partial T'}{\partial y'} = 0 \text{ at } y' = 0 \text{ and } y' = H_1, \tag{10}$$

Now introducing the stream function defined as:

$$(u', v') = (\frac{\partial \psi'}{\partial y'}, -\frac{\partial \psi'}{\partial x'}), \tag{11}$$

$$\psi = \psi' / \alpha_T, \quad t = t' \alpha_T / L_1^2, \quad \nabla = \nabla' L_1^2;$$

$$(x, x_0, y) = (x', x_0', y') / L_1, (u, v) = (u', v') L_1 / \alpha_T,$$

$$T = (T' - T_c') / (T_h' - T_c'). \tag{12}$$

The Eq. (4) takes the non − dimensional form as

$$(u, v) = (\frac{\partial \psi}{\partial y}, -\frac{\partial \psi}{\partial x}), \tag{13}$$

while the Eqs. (5) − (7) can be expressed as follows

$$\frac{\partial(\nabla^2 \psi)}{\partial t} - \frac{\partial(\psi, \nabla^2 \psi)}{\partial(x, y)} = Pr \nabla^2 (\nabla^2 \psi) \tag{14}$$

$$+ Pr(Ra_{w_0} + Ra_w)\frac{\partial T}{\partial y} - Ha^2 Pr \nabla^2 \psi.$$

$$\frac{\partial T}{\partial t} - \frac{\partial(\psi, T)}{\partial(x, y)} = \nabla^2 T. \tag{15}$$

The non-dimensional parameters, namely; Ra_{w_0}, centrifugal Rayleigh number due to offset distance; Ra_w, centrifugal Rayleigh number due to horizontal location of cavity; Prandtl number (Pr) and Hartmann number (Ha) used in above equations are defined as follows:

$$Ra_{w_0} = w^2 x_0 \beta(T_h' - T_c')L_1^2 / \upsilon \alpha_T, \tag{16}$$

$$Pr = \upsilon / \alpha_T,$$

$$Ra_w = w^2 \alpha(T_h' - T_c')L_1^3 / \upsilon \alpha_T, \tag{17}$$

$$Ha^2 = \sigma B_0^2 L_1^2 / \rho \upsilon,$$

The set of boundary conditions (8) - (10) can be shown to transform in non-dimensional form as:

$$\psi = 0 \text{ at } y = 0, Ar \text{ and at } x = 0, 1; \tag{18}$$

$$T = x \text{ at } x = 0 \text{ and at } x = 1; \tag{19}$$

$$\frac{\partial T}{\partial y} = 0 \text{ at } y = 0 \text{ and at } y = Ar. \tag{20}$$

3. TRUNCATED GALERKIN EXPANSION

To obtain the solution of the non-linear system of the partial differential Eq. (14) and (15), we represent the stream function and temperature in the form [Lorentz (1963)]:

$$\psi = A_1 \sin(\pi x) \sin(\frac{\pi y}{Ar}), \tag{21}$$

$$T = x + B_1 \sin(\pi x) \cos(\frac{\pi y}{Ar}) + B_2 \sin(2\pi x), \tag{22}$$

which is corresponding to the Galerkin expansion of the solution in both the *x*- and *y*-directions. Using Eqs. (21) and (22) in Eqs. (14) and (15) and then multiplying the equations by the corresponding orthogonal characteristic functions of Eqs. (21) and

(22) and finally integrating them over the domain $[0, 1] \times [0, Ar]$, we obtain a set of three ordinary differential equations for the time evolution of the amplitudes as:

$$\frac{dA_1(\tau)}{d\tau} = -\frac{Pr\gamma_1}{\pi^2}[\frac{\pi^2}{\gamma_1}A_1(\tau) + Ha^2 A_1(\tau) + \frac{Ra}{\pi\zeta}B_1(\tau)] \tag{23}$$

$$\frac{dB_1(\tau)}{d\tau} = -\frac{1}{\pi\zeta}A_1(\tau) - \frac{1}{\zeta}A_1(\tau)B_2(\tau) - B_1(\tau) \tag{24}$$

$$\frac{dB_2(\tau)}{d\tau} = -4\gamma_1 B_2(\tau) + \frac{1}{2\zeta}A_1(\tau)B_1(\tau) \tag{25}$$

where

$$\tau = \frac{\pi^2 t}{\gamma_1}, \ \gamma_1 = \frac{Ar^2}{Ar^2 + 1}, \ Ra = Ra_{w_0} + \frac{Ra_w}{2} \text{ and } R = \frac{Ra}{\pi^2 \zeta^2}. \tag{26}$$

If we rescale the amplitudes in the form of

$$X(\tau) = -\frac{A_1(\tau)}{2\zeta\sqrt{2\gamma_1(R-1)}}, \ Y(\tau) = \frac{\pi R B_1(\tau)}{2\sqrt{2\gamma_1(R-1)}}$$

$$\text{and } Z(\tau) = -\frac{\pi R B_2(\tau)}{R-1}, \tag{27}$$

In Eq. (23) − (25), the time is rescaled set of simultaneous differential equations:

$$\frac{dX}{d\tau} = \alpha_1[Y - \delta_2 X], \tag{28}$$

$$\frac{dY}{d\tau} = RX - Y - (R-1)XZ, \tag{29}$$

$$\frac{dZ}{d\tau} = 4\gamma_1(XY - Z). \tag{30}$$

where

$$\alpha_1 = \frac{Pr\gamma_1}{\pi^2}, \ \delta_2 = \frac{\pi^2}{\gamma_1} + Ha^2. \tag{31}$$

6.4 Stability Analyses

4.1 Dissipation

The system given by Eq. (28) − (30) is a dissipative because

$$\nabla \cdot V = \frac{\partial \dot{X}}{\partial X} + \frac{\partial \dot{Y}}{\partial Y} + \frac{\partial \dot{Z}}{\partial Z} = -[\alpha_1 \delta_2 + 1 + 4\gamma_1] < 0 \tag{32}$$

where

$$V(\tau) = V(0) \exp[-\{\alpha_1 \delta_2 + 1 + 4\gamma_1\}\tau] \tag{33}$$

The above expression clearly shows that the volume of the dynamical system decreases exponentially with the time.

4.2 Equilibrium Points

The dynamical system given by Eqs.(28)-(30) has the general form $\dot{\mathbf{X}} = f(\mathbf{X})$ and the equilibrium (fixed or stationary) points $\mathbf{X_s}$ are given by $f(\mathbf{X_s}) = \mathbf{0}$ the equilibrium points of the rescaled system are

$$(X_1, Y_1, Z_1) = (0, 0, 0), \tag{34}$$

Corresponding to the motionless solution and

$$X_2, X_3 = \pm\sqrt{\frac{R - \delta_2}{(R-1)\delta_2}}, \tag{35}$$

$$Y_2, Y_3 = \pm\sqrt{\frac{[R - \delta_2]\delta_2}{R-1}}, \tag{36}$$

$$Z_2 = Z_3 = \frac{R - \delta_2}{R - 1}, \tag{37}$$

corresponding to the convection solution.

4.3 Stability of Equilibrium Points

The Jacobian matrix of the system of Eqs.(28)-(30) is obtained as follows:

$$J = \begin{bmatrix} -\alpha_1\delta_2 & \alpha_1 & 0 \\ R - (R-1)Z & -1 & (R-1)X \\ 4\gamma_1 Y & 4\gamma_1 X & -4\gamma_1 \end{bmatrix}. \tag{38}$$

The eigenvalues of the Jacobian matrix obtained by solving the zeros of the Characteristic polynomial provide the stability conditions. A fixed point is stable if all the real eigenvalues are negative. But in the case of complex eigenvalues, a fixed point is stable if the real parts of them are negative. However, a fixed point is not stable when at least one eigenvalue becomes positive (or in the case of complex eigenvalues, it has positive real part).

The stability of the fixed point $X_1 = 0, Y_1 = 0, Z_1 = 0$ corresponding to the motionless solution is controlled by the zeros of the following characteristic polynomial equation for the eigenvalues $\chi_i (i = 1, 2, 3)$:

$$(4\gamma_1 + \chi)\big[\alpha_1 R - (1 + \chi)(\alpha_1\delta_2 + \chi)\big] = 0. \tag{39}$$

The eigenvalue of the Eq. 39 are obtained as

$$\chi_1 = -4\gamma_1, \tag{40}$$

$$\chi_2, \chi_3 = \frac{1}{2}[-(\alpha_1\delta_2 + 1)$$

$$\pm\sqrt{(\alpha_1\delta_2 + 1)^2 + 4\alpha_1(R - \delta_2)}\;] \tag{41}$$

We can see that the eigenvalues χ_1 and χ_3 are always negative as $\gamma_1 > 0$ and the eigenvalue χ_2 provides only the stability condition for the motionless solution in the form $R < \delta_2$. Therefore, the critical value of R, where the motionless solution loses stability and the convection solution (expressed by the other two fixed points) take over, is determined as:

$$R_c = R_{cr} = \delta_2, \quad or \quad Ra_{cr} = 4\pi^2\delta_2. \tag{42}$$

The stability of the fixed points corresponding to the convection solution (X_2, Y_2, Z_2) and (X_3, Y_3, Z_3) is controlled by the following equation:

$$\delta_2\chi^3 + \delta_2\big[\alpha_1\delta_2 + 4\gamma_1 + 1\big]\chi^2$$

$$+\Big[4\gamma_1(\delta_2^2 + R)\Big]\chi + \delta_2\big[8\alpha_1\gamma_1(R - \delta_2)\big] = 0. \tag{43}$$

Equation. 43 yields three eigenvalues, all the roots are real and negative at slightly supercritical value of

R and the convection fixed points are stable. Thus, the fixed points are simple nodes. These roots move on the real axis towards the origin as the value of R increases. These roots move on the real axis toward

the origin as the value of R increases. These roots become equal when

$$R = \frac{\alpha_1\delta_2^2[\alpha_1\delta_2 + 4\gamma_1 + 3]}{\alpha_1\delta_2 - 4\gamma_1 - 1}. \tag{44}$$
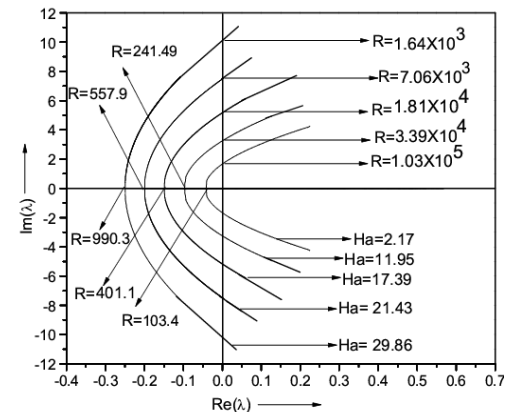
**Fig. 2. Variation in eigenvalues on Agrand diagram with *Ha* and *R*.**

Fig. 2. shows that at $Ha = 2.17, 11.95, 17.39, 21.43$ and $29.86.$, both roots χ_2, χ_3 are purely real, negative and equal. When we take the slightly supercritical value of R, the roots become complex conjugate with negative real part and further on increasing the value of R, they are approaching towards the origin on the real axis. They have still negative real parts and therefore, the convection fixed points are stable i.e. spiral nodes. Corresponding to the Hartmann Number $Ha = 2.17, 11.95, 17.39, 21.43$ and $29.86.$, the roots become purely imaginary i.e. their real parts becomes zero at $R = 1.64 \times 10^3, 7.06 \times 10^3, 1.81 \times 10^4, 3.39 \times 10^4$ and 1.03×10^5 (listed in Table 1). Again on increasing the value of R, both the imaginary and the real parts of these two complex conjugate eigenvalues increase and on the complex plane, they cross the imaginary axis *i.e* their real part becomes positive and motion is

Table 1 Values of R where $\lambda_2 = \lambda_3$ (when the loss of stability occurred for the different values of *Ha*)

Ha	In Motionless State		In Convective Motion	
	R	Ra	R	Ra
2.17	103.40	1.13×10^4	1.64×10^3	1.80×10^5
11.95	241.49	2.64×10^4	7.06×10^3	7.75×10^5
17.39	401.10	4.39×10^4	1.81×10^4	1.98×10^6
21.43	557.94	6.11×10^4	3.39×10^4	3.71×10^6
29.86	990.31	1.09×10^5	1.03×10^5	1.13×10^7
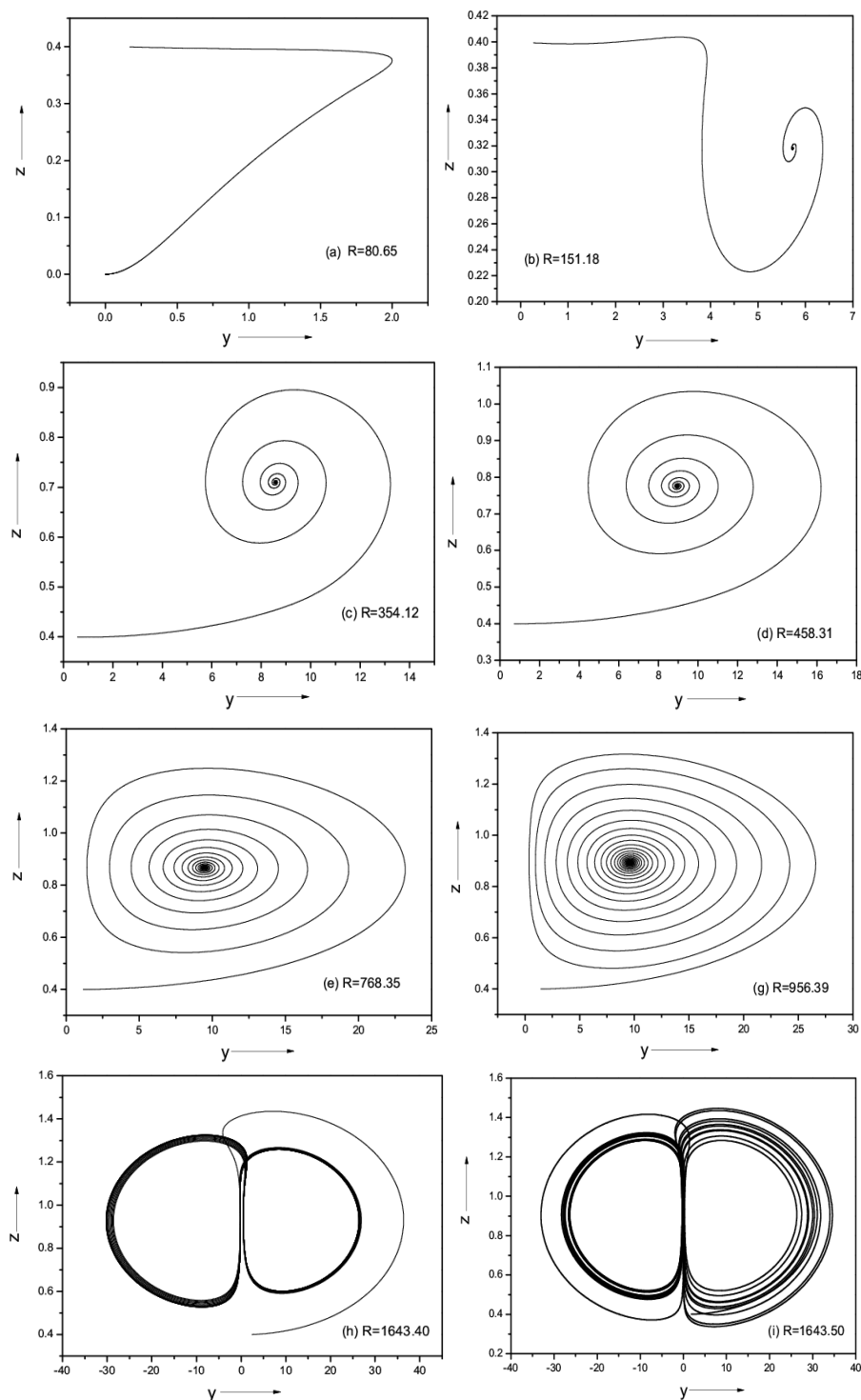
Fig. 3. Evolution of trajectories at *Ha*=2.17 for different values of *R*.
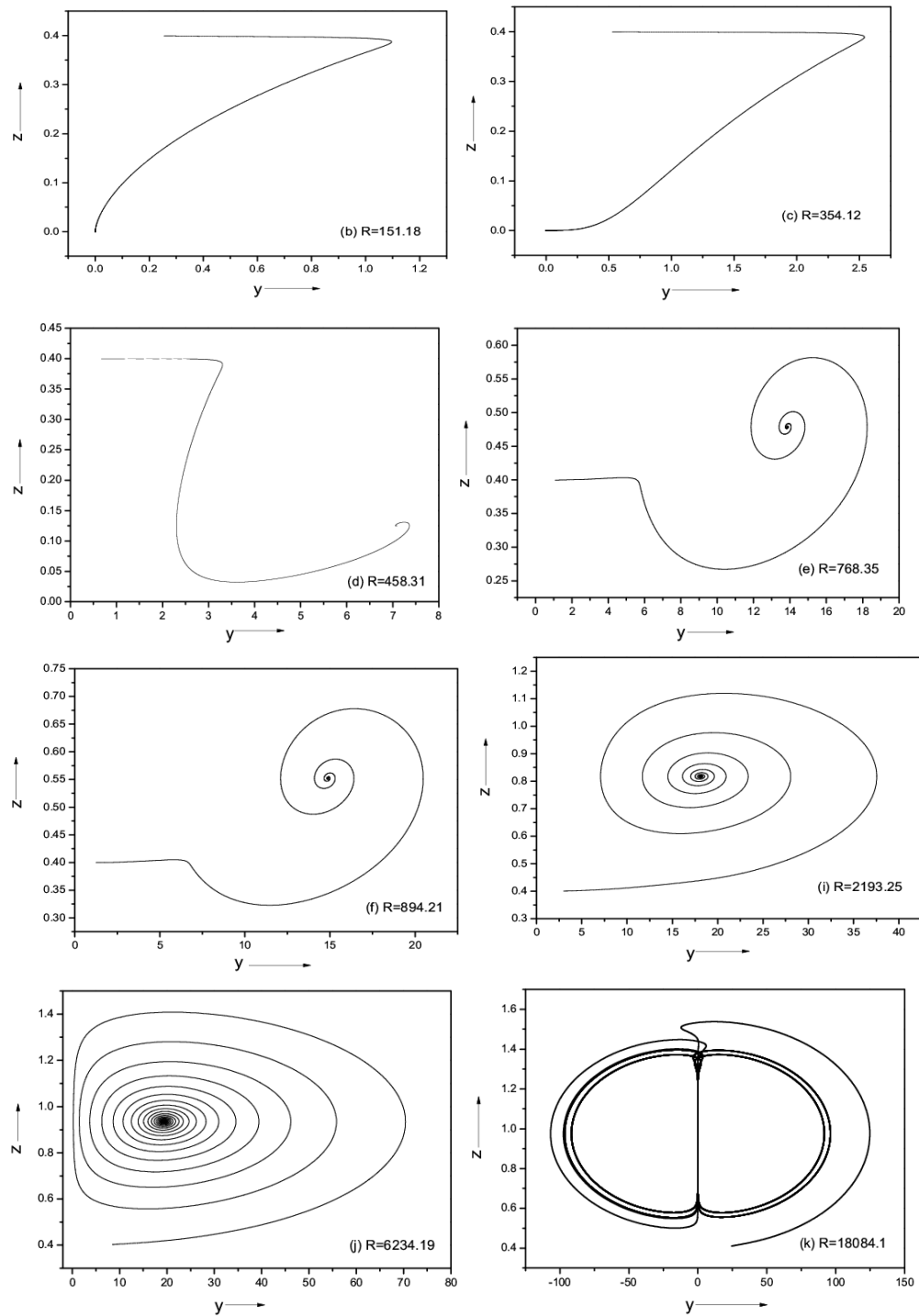
Fig. 4. Evolution of trajectories at *Ha*=17.39 for different values of *R*.

unstable. In Table 1, we have listed the values of R for different values of Ha.

4.3 Heat Transport

From engineering point of view, one of the important characteristic of the flow is to see the effect of physical parameters on the rate of heat transfer across the cavity, and this is obtained by computing the values of the Nusselt number, Nu.

The local Nusselt number on the horizontal bottom of the cavity is obtained by

$$Nu = (\frac{\partial T}{\partial x})_{x=0} = 1 + \pi B \cos(\frac{\pi y}{Ar}) + 2\pi B_2. \qquad (45)$$

The overall heat transfer rate across the cavity, expressed by the average Nusselt number at the horizontal bottom, is obtained by using the
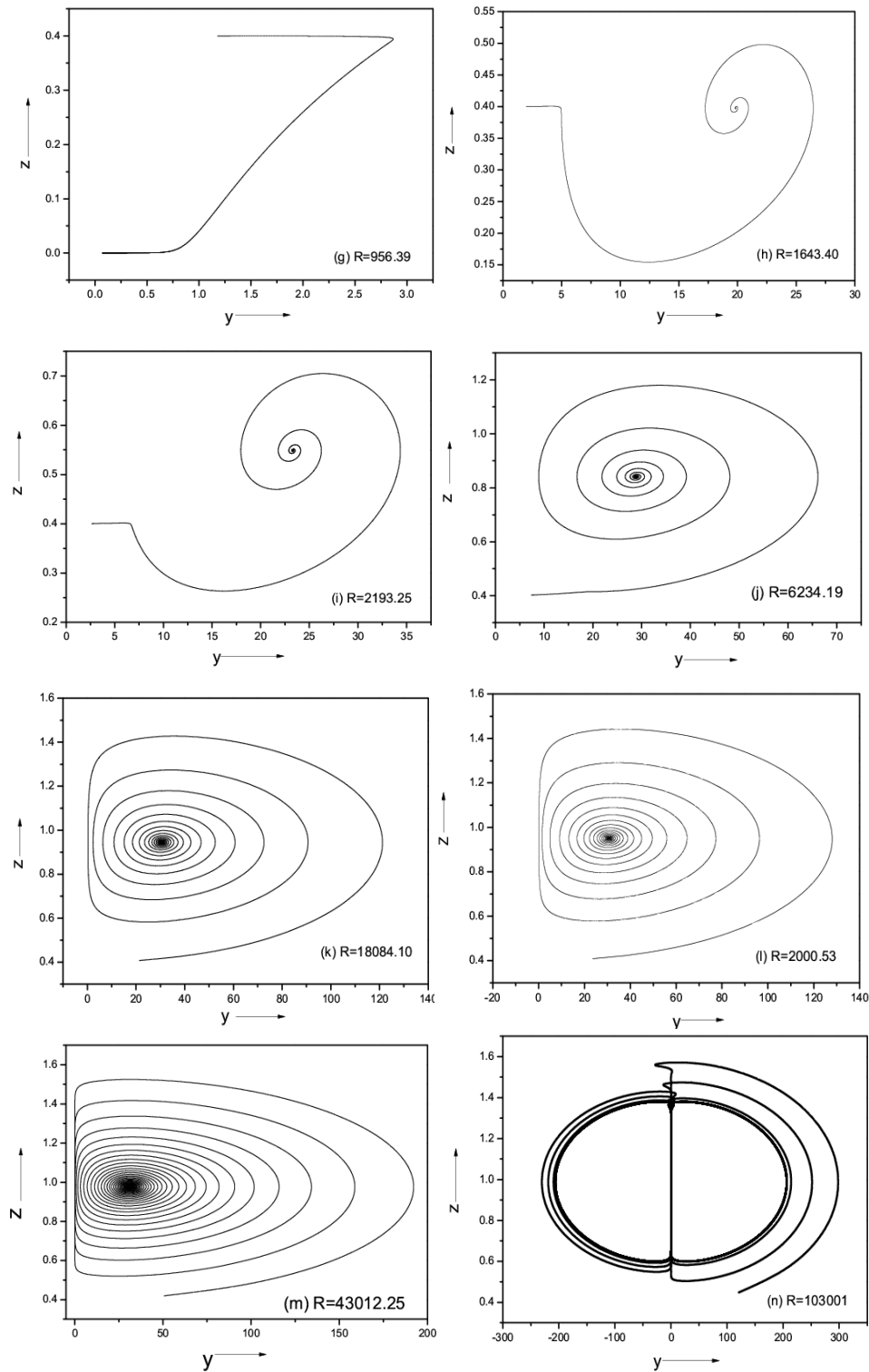
Fig. 5. Evolution of trajectories at *Ha*=29.86 for different values of *R*.

following relation:

$$Nu_{av}\big|_{x=0}=\frac{1}{A_r}\int_0^{A_r}Nudy.$$

(46)

Using Eqs. (22) and (45) in Eq. (46), we get

$$Nu_{av}\big|_{x=0}=1+2\pi B_2=1+\frac{2(1-R)}{R}Z.$$

(47)

5. RESULT AND DISCUSSION

In order to see the dynamic behavior of the system,

we present some numerical simulations of the system of Eqs. (28)-(30) for the time domain $0 \leq \tau \leq 80$. All the calculations are performed by using the Runge-Kutta method of fourth- order on double precision when the time step is 0.005, by fixing the values $\alpha_1 = 0.1$, $\gamma_1 = 0.1$ and taking the common initial conditions as X(0) = 0.5, $Y(0)$ = 0.05, $Z(0)$ = 0.4 in the neighbourhood of the positive convective fixed point. Here, we shall demonstrate different possible solutions and transition values of R and Ha for the fixed value of α_1 and γ_1.

The evolution of trajectories over time in the state space for increasing values of scaled Rayleigh number is presented in Fig. 3, in terms of the projections of trajectories onto the $Y — Z$ plane for $Ha = 2.17$. From Fig. 3a, it is evident that the trajectory is like a concave curve with respect to the z-axis and moving to the steady convection point starting from initial point (0.5, 0.05, 0.4) for $R = 80.65$ i.e. the convection solution is a stable simple node. The motionless solution losses its stability for a Rayleigh number slightly above $Rc_1 = 103.4$ In Fig. 3b, For $R = 151.18$ the solution shows that the trajectory is attracted to the convective fixed point via a spiral i.e. the fixed point is a stable spiral node, which predicated a transition of the two originally real roots to a pair of complex conjugate roots at a value of R_{c1} = 103.40.

Fig. 3c, 3d, 3e and 3g show that for higher values of R i.e. $R = 354.12$, $R = 458.31$, $R = 768.35$ and $R = 956.39$, the spiraling approach of the trajectories towards the fixed point becomes faster. For $R = 1643.40$ and $R = 1643.50$, the real part of the of complex conjugate eigen-values becomes positive and hence the convective fixed points losses their stability and it can be seen in Fig. 3h and 3i in which the transition to chaotic solution occurs.

In Fig. 4, we have presented the evolution of trajectories over time in the state space for increasing values of the scaled Rayleigh number at $Ha = 17.39$ in terms of the projections of trajectories onto the Y- Z plane. It is evident from Figs. 4b and 4c that the trajectory is a concave curve with respect to the $z—axis$ and moving to the steady convection point starting from initial point (0.5, 0.05, 0.4) for $R = 80.65$, $R = 151.18$ and $R = 354.12$ respectively and thus, the convection solution is a stable simple node. In this case, the motionless solution losses its stability for the Rayleigh number slightly above $Rc_1 = 401.10$. Figs. *4d*, *4e*, and *4f* for $R = 458.31$, $R = 768.35$, $R = 894.21$ and $R = 956.39$ respectively show that the trajectory is attracted to the convective fixed point in the form of a spiral. It shows that the fixed point is a stable spiral node. Further, from Figs. *4i* and *4j*

at $R = 2193.25$ and $R = 6234.19$ respectively, we can see that the trajectories approach to the convective fixed point on a spiral and the closeness of spiraling near the fixed point increase on increasing

the value of R i.e. the stability of the convective fixed point increases by increasing the value of R. Fig. *4k* at $R = 18084.10$ clearly indicates that a limit cycle is created i.e. the solution is not heading any more towards the convective fixed point but rather fluctuates periodically around it. Also it (when the real part of the pair of complex conjugate eigenvalues become positive) shows that the convective fixed points lose their stability i.e. chaotic solution occurs.

When $Ha = 29.86$, we found that at $Rc_1 = 990.3$, the motionless solution loses stability and the convection solution occurs. For $R = 1.03$ x 10^5, the convection fixed points lose their stability and a chaotic solution takes over. The evolution of trajectories over time in the state space for increasing values of the scaled Rayleigh number is presented in Fig. 5 in terms of the projections of trajectories onto the Y- Z plane. From Fig. 5g, it is evident that the trajectory is like a concave curve w.r.t the $z-axis$ and moving to the steady convection point starting from initial point $(0.05, 0.5, 0.9)$ for $R = 80.65, 151.18, 354.12, 458.31, 768.35, 894.21$ and 956.39 respectively i.e the convection solution is a stable simple node. The motionless solution losses its stability for a Rayleigh number slightly above $Rc_1 = 990.31$. For $R = 1643.40$, Fig. 5h shows that the trajectory is attracted to the convective fixed point via a spiral i.e. the fixed point is a stable spiral node, which predicated a transition of the two originally real roots to a pair of complex conjugate roots at a value of $Rc_1 = 990.31$.

At $R = 43012.25$ the spiraling approach increases towards the fixed point and closeness also increases than $R = 2000.53, 18084.10, 6234.19, 2193.25$ as shown in Figs. 5m, 5l, 5k, 5j and 5i respectively. At the value of $R = 10300.1$, we obtain a solitary limit cycle indicating the loss of stability of the convection fixed points (Fig. 5n. We can observe in Fig. 5n that the transition to chaotic solution occurs at a value greater than critical value of $R = 1.03$ x 10^5.
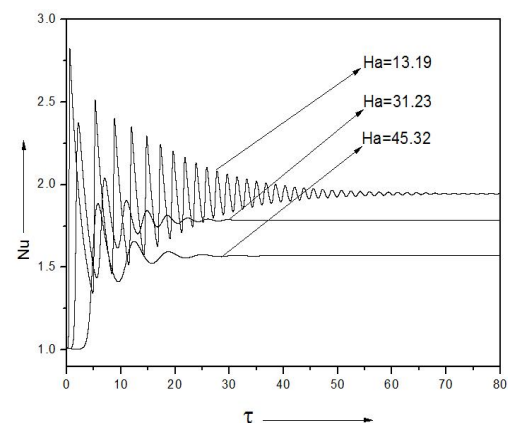
Fig. 6. Variation in Nusselt number Nu with respect to time τ for different values of the Hartmann number Ha at $R = 5.13$ x 10^5.

Fig. 6 shows the plots of the Nusselt number Nu with respect to time τ for different values of the Hartmann number Ha at $R = 5.13 \times 10^5$. We observed that initially when τ is small, the value of Nu oscillates and finally approaches to a steady state by assuming a constant value. Also, it is clear that Nu approaches to its steady state at $\tau =$ 27.305, 29.975, 74.03 for $Ha = 45.32, 31.23, 13.19$ respectively i.e. the convection become slower on increasing Ha. It means that the convection becomes stable with Ha.
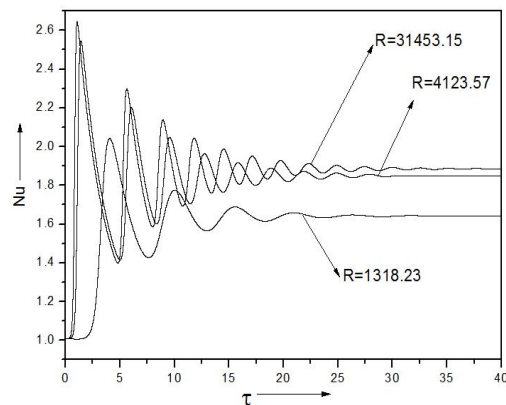
Fig. 7. Variation in Nusselt number Nu with respect to time τ at $Ha = 19.31$, for different values of the scaled Rayleigh number R.

Fig. 7 shows the plots of Nusselt number Nu with respect to time τ at $Ha = 19.31$, for different values of the scaled Rayleigh number R. We observed that initially when τ is small, the value of Nu oscillates and finally approaches to steady state by assuming constant value. Also, it clear that Nu approaches to its steady state value at $\tau =$ 21.985000, 30.115000, 35.780000 for $R = 1318.23$, 4123.57, 31453.15 respectively i.e. the convection become faster on increasing R. It means that the convection is unstable with R.

6. CONCLUSIONS

In this work, we have investigated the effect of a transverse magnetic field on chaos in a rotating cavity subject to the centrifugal acceleration and heated from side. Our results demonstrate different transitions, e.g. from steady convection to a non-periodic regime via a Hopf bifurcation and a further transition from chaos to periodic convection at significantly higher values of the scaled Rayleigh number. We found that there is inversely proportional relation between the Hartmann number Ha and scaled Rayleigh number R. This results provide evidence that the presence of a magnetic field delay the convection motion on chaos in a rotating cavity i.e the system is more stable.

REFERENCE

Bekki, N. and H. Moriguchi (2007). Temporal chaos in Boussinesq magnetoconvection. *Phys. Plasmas 14, Art. no. 012306.*

Chandrasekhar, S. (1952). Hydrodynamic and Hydromagnetic Stability, (Clarendon, Oxford, 1961). *Philosophical Magazine 43, 146.*

Chen, Z. M. and W. G. Price (2006). On relation between Rayleigh- Benard convection and Lorenz system. *Chaos Solitons Fractals 28, 571-578.*

Cox, S. M. and P. C. Matthews (2001). New instabilities in two-dimensional rotating convection and magnetoconvection. *Physica D 149, 210-229.*

Das, S. S., S. R. Biswal, U. K. Tripathy and P. Das (2011). Mass Transfer Effects on Unsteady Hydromagnetic Convective Flow past Vertical Porous Plate in a Porous Medium with Heat Source. *Journal of Applied Fluid Mechanics* 4(4), 91-100.

Garandet, J. P., T. Alboussiere and R. Moreau (1992). Buoyancy driven convection in a rectangular enclosure with a transverse magnetic field. *International Journal of Heat and Mass Transfer 35, 741-748.*

Gelfgat, A. Y. and P. Z. Yoseph (2001). The effect of an external magnetic field on oscillatory instability of convective flows in a rectangular cavity. *Physics of Plasmas 13, 2269-2278.*

Ghosh, S. K., G. C. Shit and J. C. Misra (2014). Heat Transfer in Hydromagnetic Fluid Flow: Study of Temperature Dependence of Fluid Viscosity. *Journal of Applied Fluid Echanics* 7(4), 633-640.

Govender, S. (1995). *Stability analysis of free convection in rotating porous media subject to centrifugal and gravitational body forces.* M.Sc. thesis, University of Durban- Westville.

Greenspan, H. P. (1980). *The Theory of Rotating Fluids.* Cambridge Univ. Press, Cambridge 5-18.

Gupta, V. K., R. Prasad and A. K. Singh (2013). Effect of magnetic field on chaos in couple stress liquid saturated porous layer. *IJET* 5(28), 1-9.

Kandaswamy, P., S. Malliga Sundari and N. Nithyadevi (2008). Magnetoconvection in an enclosure with partially active vertical walls. *International Journal of Heat and Mass Transfer 51, 1946-1954.*

Knobloch, E. and N. O. Weiss (1983). Birfucations in a model of magnetoconvection. *PhysicaD: Nonlinear Phenomena 9(3), 379-407.*

Knobloch, E., D. R. Moore, J. Toomre and N. O. Weiss (1986). Transitions to chaos in two-dimensional double-diffusive convection. *Journal of Fluid Mechanics 166, 409-448.*

Knobloch, E., N. O. Weiss and L. N. Costa (1981). Oscillatory and steady convection in a

magnetic field. *Journal of Fluid Mechanics 113, 153-186.*

Kumar, P. (2012). Thermosolutal Magneto – Rotatory Convection in Couple - Stress Fluid through Porous Medium. *Journal of Applied Fluid Mechanics* 5(4), 45-52.

Lorenz, E. N. (1963). Deterministic nonperiodic flow. *Journal of the Atmospheric Sciences 20(2), 130-141.*

Matsuba, K., K. Imai and K. Nozaki (1997). Nonlinear modulation of travelling rolls in magnetoconvection. *Physica D 107, 69-74.*

Nithyadevi, N., P. Kandaswamy and J. Lee (2007). Natural convection in a rectangular cavitywith partially active side walls. *International Journal of Heat Mass Transfer 50, 4688-4697.*

Prasad, R. and A. K. Singh (2013). Effect of perpendicular magnetic field on chaos in a cavity heated from below. *International Journal of applied Mathematics and informatics 7, 85-96.*

Reddy, T. S., M. C. Raju and S. V. K. Varma (2013). Unsteady MHD Radiative and Chemically Reactive Free Convection Flow near a Moving Vertical Plate in Porous Medium. *Journal of Applied Fluid Mechanics* 6(3), 443-451.

Rucklidge, A. M. (1992). Chaos in models of double convection. *Journal of Fluid Mechanics 237, 209-229.*

Rucklidge, A. M. (1993). Chaos in a low-order model of magnetoconvection. *Physica D 62, 323-337.*

Rucklidge, A. M. (1994). Chaos in magnetoconvection. *Nonlinearity 7, 1565-1591.*

Rucklidge, A. M., N. O. Weiss, D. P. Brownjohn, P. C. Matthews and M. R. E. Proctor (2000). Compressible magnetoconvection in three dimensions: pattern formation in a strongly stratified layer. *Journal of Fluid Mechanics 419, 283-323.*

Sharma, B. R. and K. Nath (2015). Demixing of a Binary Fluid Mixture in Case of MHD Flow with Heat and Mass Transfer due to a Point. Sink. *Journal of Applied Fluid Mechanics*, Vol. 8, No. 4, pp. 661-665.

Vadasz, P. (1996). Stability of free convection in a rotating porous layer distance from the axis rotation. *Transport in porous media 23, 153-173.*

Vadasz, P. (1998). Transitions and chaos for free convection in a rotating porous layer. *Internatonal Journal of Heat Mass Transfer 41, 1417-1435.*

Veerraju, N., K. S. Srinivasa Babu and C. N. B. Rao (2012). Mixed Convection at a Vertical Plate in a Porous Medium with Magnetic Field and Variable Viscosity. *Journal of Applied Fluid Mechanics* 5(4), 53-62.

Weiss, N. O. (1981). Numerical simulations of partial differential equation for two dimensional Boussinesq magnetoconvection and aperiodic behavior to regular oscillations. *Journal of Fluid Mechanics 108, 247.*